



ELSEVIER

Available online at www.sciencedirect.com

SCIENCE @ DIRECT®

International Journal of Pressure Vessels and Piping 81 (2004) 635–644

INTERNATIONAL JOURNAL OF
Pressure Vessels
and Piping

www.elsevier.com/locate/ijpvp

Variations of stress intensity factors of a semi-elliptical surface crack subjected to mode I, II, III loading

Nao-Aki Noda*, Masayuki Kagita

Department of Mechanical Engineering, Kyushu Institute of Technology, 1-1, Sensui-cho, Tobata, Kitakyushu 804-8550, Japan

Received 10 October 2003; revised 22 March 2004; accepted 22 March 2004

Abstract

Maximum stress intensity factors of a surface crack usually appear at the deepest point of the crack, or a certain point along the crack front near the free surface depending on the aspect ratio of the crack. However, generally it has been difficult to obtain smooth distributions of stress intensity factors along the crack front accurately due to the effect of a corner point singularity. It is known that the stress singularity at a corner point where the front of a three-dimensional (3D) crack intersects a free surface depends on Poisson's ratio and is different from the ordinary crack singularity. In this paper, a singular integral equation method is applied to calculate the stress intensity factor along the crack front of a 3D semi-elliptical surface crack in a semi-infinite body under mode I, II, III loading. The body force method is used to formulate the problem as a system of singular integral equations with singularities of the form r^{-3} using the stress field induced by a force doublet in a semi-infinite body as a fundamental solution. In the numerical calculation, unknown body force densities are approximated by using fundamental density functions and polynomials. The results show that the present method yields smooth variations of mode I, II, III stress intensity factors along the crack front accurately. Distributions of stress intensity factors are indicated in tables and figures as functions of the elliptical shape and Poisson's ratio.

© 2004 Published by Elsevier Ltd.

Keywords: Elasticity; Stress intensity factor; Body force method; Semi-elliptical surface crack; Singular integral equation; Numerical analysis

1. Introduction

Semi-elliptical surface cracks lying perpendicular to the surface in Fig. 1 have been used as a fundamental model for actual defects. Here, an elliptical crack is also considered as an internal defect to clarify the effect of free surface. In three-dimensional (3D) surface cracks the point where the crack front intersects a free surface is known as a corner point. Several researchers discussed that the stress singularity at this point is different from that of an ordinary crack, that is, $r^{-0.5}$. With r as the distance from the corner point, the singular stresses associated with the symmetric field (mode I) become unbounded as r diminishes according to $\sigma \propto r^{-\lambda_S}$ while the stresses in the anti-symmetric fields (modes II and III) satisfy $\sigma \propto r^{-\lambda_A}$ (see Fig. 2). Fig. 3 and Tables 1a and 1b indicate the values of the corner point singularities λ_S and λ_A , respectively [1–8]. Then, the singular indices vary in the range $0.5 \geq \lambda_S \geq 0.332$ for

symmetric deformations, and in the range $0.5 \leq \lambda_A \leq 0.646$ for skew-symmetric deformations, depending on Poisson's ratio in the range $0 \leq \nu \leq 0.5$. Generally, it has been difficult to obtain smooth distributions of stress intensity factors along the crack front accurately because of the effect of the corner point singularity.

In our previous studies, the body force method was used to formulate 3D crack problems as a system of integral equations. In the numerical solutions, unknown body force densities were approximated by using fundamental density functions and polynomials. Then, the method was found to yield highly satisfied boundary conditions [9,10]. In this paper, the method is applied to calculate the stress intensity factor along the crack front of a 3D semi-elliptical surface crack under the three types of loading shown in Fig. 1. The present method is efficient and useful for obtaining accurate and smooth variations of mode I, II, III stress intensity factors even very close to the free surfaces where the effect of the corner point singularities appears. Distributions of stress intensity factors will be indicated in tables and figures for varying elliptical shape and Poisson's ratio.

* Corresponding author. Tel.: +81-93-884-3124; fax: +81-93-884-3124.
E-mail address: noda@mech.kyutech.ac.jp (N.-A. Noda).

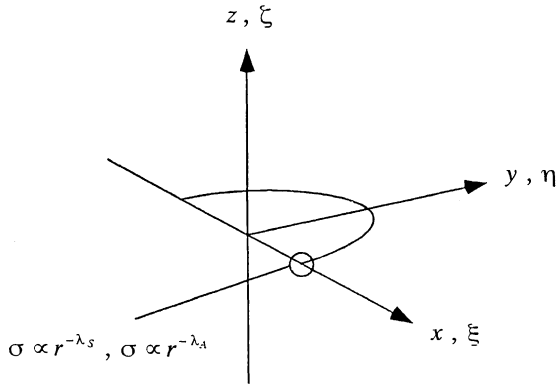


Fig. 2. Stress singularity at the corner point.

Here, Eqs. (1a)–(1d) include singular terms in the form $1/r_1^3$, $1/r_1^5$ corresponding to those of an elliptical crack in an infinite body. The notation \iint_S should be interpreted as a finite part integral in the region S . The notation $K_{yz}^{f_{yz}}(\xi, \eta, x, y)$ refers to a function that satisfies the boundary condition for a free surface

$$\begin{aligned} & \frac{1-2\nu}{8\pi(1-\nu)^2} \left[\iint_S \frac{f_{zz}(\xi, \eta)}{r_1^3} d\xi d\eta \right. \\ & + \left. \iint_S K_{zz}^{f_{zz}}(\xi, \eta, x, y) f_{zz}(\xi, \eta) d\xi d\eta \right] \\ & + \frac{1}{8\pi(1-\nu)} \left[\iint_S K_{zz}^{f_{yz}}(\xi, \eta, x, y) f_{yz}(\xi, \eta) d\xi d\eta \right. \\ & + \iint_S K_{yz}^{f_{yz}}(\xi, \eta, x, y) f_{yz}(\xi, \eta) d\xi d\eta \\ & + \left. \iint_S K_{yz}^{f_{zx}}(\xi, \eta, x, y) f_{zx}(\xi, \eta) d\xi d\eta \right] \\ & = p_{zz}(x, y) \end{aligned} \tag{1a}$$

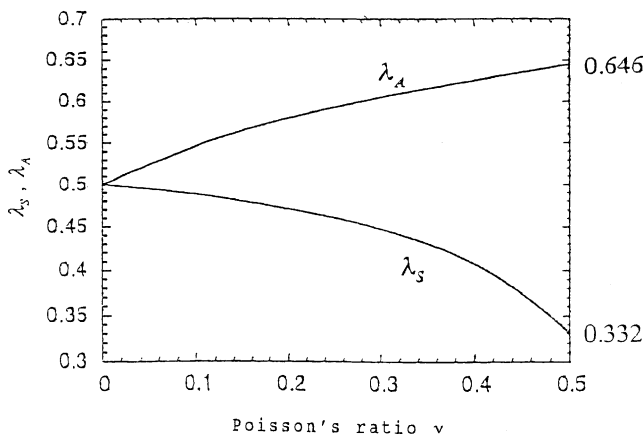


Fig. 3. Singular indices at the corner point.

Table 1a
Singular indices at the corner point, λ_s of mode I deformation

ν	Ref. [1]	Ref. [2]	Ref. [3]	Ref. [4]
0	0.5	0.49997		0.5002
0.1				0.4904
0.15	0.4836	0.4835	0.484	
0.2				0.4755
0.3	0.4523	0.4519	0.452	0.4523
0.4	0.4132	0.4141	0.413	0.4133
0.5	0.3318	0.3452		0.3316

$$\begin{aligned} & \frac{1}{8\pi(1-\nu)} \left[\iint_S \left\{ \frac{2(1-2\nu)}{r_1^3} + \frac{6\nu(y-\eta)^2}{r_1^5} \right\} f_{yz}(\xi, \eta) d\xi d\eta \right. \\ & + \iint_S \frac{6\nu(x-\xi)(y-\eta)}{r_1^5} f_{zx}(\xi, \eta) d\xi d\eta \\ & + \iint_S K_{yz}^{f_{zz}}(\xi, \eta, x, y) f_{zz}(\xi, \eta) d\xi d\eta \\ & + \iint_S K_{yz}^{f_{yz}}(\xi, \eta, x, y) f_{yz}(\xi, \eta) d\xi d\eta \\ & + \left. \iint_S K_{yz}^{f_{zx}}(\xi, \eta, x, y) f_{zx}(\xi, \eta) d\xi d\eta \right] = p_{yz}(x, y) \end{aligned} \tag{1b}$$

$$\begin{aligned} & \frac{1}{8\pi(1-\nu)} \left[\iint_S \frac{6\nu(x-\xi)(y-\eta)}{r_1^5} f_{yz}(\xi, \eta) d\xi d\eta \right. \\ & + \iint_S \left\{ \frac{2(1-2\nu)}{r_1^3} + \frac{6\nu(x-\xi)^2}{r_1^5} \right\} f_{zx}(\xi, \eta) d\xi d\eta \\ & + \iint_S K_{zx}^{f_{zz}}(\xi, \eta, x, y) f_{zz}(\xi, \eta) d\xi d\eta \\ & + \iint_S K_{zx}^{f_{yz}}(\xi, \eta, x, y) f_{yz}(\xi, \eta) d\xi d\eta \\ & + \left. \iint_S K_{zx}^{f_{zx}}(\xi, \eta, x, y) f_{zx}(\xi, \eta) d\xi d\eta \right] = p_{zx}(x, y) \end{aligned} \tag{1c}$$

$$\begin{aligned} & r_1 = \sqrt{(x-\xi)^2 + (y-\eta)^2 + (z-\zeta)^2} \\ & S = \{(\xi, \eta) | (\xi/a)^2 + (\eta/b)^2 \leq 1, \eta \geq 0\} \end{aligned} \tag{1d}$$

In the present analysis, the following expressions have been used to approximate the unknown functions $f_{zz}(\xi, \eta)$,

Table 1b
Singular indices at the corner point, λ_A of mode II, III deformation

ν	Ref. [2]	Ref. [3]
0	0.4999	
0.15	0.5668	0.565
0.3	0.6073	0.598
0.4	0.6286	0.604
0.5	0.6462	

$f_{yz}(\xi, \eta), f_{zx}(\xi, \eta)$ as continuous functions [9]:

$$\left. \begin{aligned}
 f_{zz}(\xi, \eta) &= F_{zz}(\xi_a, \eta_b)w_{zz}(\xi_a, \eta_b) \\
 f_{yz}(\xi, \eta) &= F_{yz}(\xi_a, \eta_b)w_{yz}(\xi_a, \eta_b) \\
 f_{zx}(\xi, \eta) &= F_{zx}(\xi_a, \eta_b)w_{zx}(\xi_a, \eta_b) \\
 w_{zz}(\xi_a, \eta_b) &= \frac{4(1-\nu)^2 b \sigma_z^\infty}{(1-2\nu)E(k)} \sqrt{1-\xi_a^2-\eta_b^2}, \sigma_z^\infty = 1 \\
 w_{yz}(\xi_a, \eta_b) &= \frac{2b(1-\nu)k^2 \tau_{yz}^\infty}{C(k)} \sqrt{1-\xi_a^2-\eta_b^2}, \tau_{yz}^\infty = 1 \\
 w_{zx}(\xi_a, \eta_b) &= \frac{2b(1-\nu)k^2 \tau_{zx}^\infty}{B(k)} \sqrt{1-\xi_a^2-\eta_b^2}, \tau_{zx}^\infty = 1 \\
 B(k) &= (k^2-\nu)E(k) + \nu k'^2 K(k) \\
 C(k) &= (k^2 + \nu k'^2)E(k) - \nu k'^2 K(k) \\
 k' &= b/a \leq 1, k = \sqrt{1-(b/a)^2}, \xi_a = \xi/a, \eta_b = \eta/b \\
 K(k) &= \int_0^{\pi/2} \frac{d\lambda}{\sqrt{1-k^2 \sin^2 \lambda}}, E(k) = \int_0^{\pi/2} \sqrt{1-k^2 \sin^2 \lambda} d\lambda
 \end{aligned} \right\} \quad (2)$$

Here, $w_{zz}(\xi_a, \eta_b), w_{yz}(\xi_a, \eta_b), w_{zx}(\xi_a, \eta_b)$ are called fundamental density functions, which express the stress field due to an elliptical crack in an infinite body under stresses $\sigma_z^\infty, \tau_{yz}^\infty, \tau_{zx}^\infty$ and lead to solutions with high accuracy. Using expression (2), Eq. (1b) is reduced to Eq. (3) below, where unknown functions $F_{zz}(\xi_a, \eta_b), F_{yz}(\xi_a, \eta_b), F_{zx}(\xi_a, \eta_b)$ are called weight functions

$$\begin{aligned}
 &\frac{b}{4\pi} \left[\frac{k^2}{C(k)} \iint_S \left\{ \frac{2(1-2\nu)}{r_1^3} + \frac{6\nu(y-\eta)^2}{r_1^5} \right\} F_{yz}(\xi_a, \eta_b) \right. \\
 &\quad \times \sqrt{1-\xi_a^2-\eta_b^2} d\xi d\eta + \frac{k^2}{B(k)} \iint_S \frac{6\nu(x-\xi)(y-\eta)}{r_1^5} \\
 &\quad \times F_{zx}(\xi_a, \eta_b) \sqrt{1-\xi_a^2-\eta_b^2} d\xi d\eta + \frac{2(1-\nu)}{(1-2\nu)E(k)} \\
 &\quad \times \int \int_S K_{yz}^{f_{yz}}(\xi, \eta, x, y) F_{zz}(\xi_a, \eta_b) \sqrt{1-\xi_a^2-\eta_b^2} d\xi d\eta \\
 &\quad + \frac{k^2}{C(k)} \int \int_S K_{yz}^{f_{yz}}(\xi, \eta, x, y) F_{yz}(\xi_a, \eta_b) \sqrt{1-\xi_a^2-\eta_b^2} d\xi d\eta \\
 &\quad \left. + \frac{k^2}{B(k)} \int \int_S K_{yz}^{f_{zx}}(\xi, \eta, x, y) F_{zx}(\xi_a, \eta_b) \sqrt{1-\xi_a^2-\eta_b^2} d\xi d\eta \right] \\
 &= p_{yz}(x, y) \quad (3)
 \end{aligned}$$

In the previous studies, the problems $p_{zz}=p_0, p_{zx}=p_0$ were considered [9,10]. In this study, consider an elliptical crack subjected to shear loading in the y-direction assuming $p_{yz}=p_0(y/b)$, and also $p_{yz}=p_0$ ($p_{zz}=p_{zx}=0$) in order to compare with the solution of an elliptical crack subjected to

uniform shear. Since Fig. 1(c) is symmetric with respect to the y-axis, the expression (4) can be applied to approximate unknown functions $F_{zz}(\xi_a, \eta_b), F_{yz}(\xi_a, \eta_b), F_{zx}(\xi_a, \eta_b)$.

$$\left. \begin{aligned}
 F_{zz}(\xi_a, \eta_b) &= \alpha_0 + \alpha_1 \eta_b + \dots + \alpha_{n-1} \eta_b^{n-1} + \alpha_n \eta_b^n + \alpha_{n+1} \xi_a^{2 \times 1} \\
 &\quad + \alpha_{n+2} \xi_a^{2 \times 1} \eta_b + \dots + \alpha_{2n} \xi_a^{2 \times 1} \eta_b^{n-1} + \dots \\
 &\quad + \alpha_{l-2} \xi_a^{2(n-1)} + \alpha_{l-1} \xi_a^{2(n-1)} \eta_b + \alpha_l \xi_a^{2n} \\
 &= \sum_{i=0}^l \alpha_i G_i(\xi_a, \eta_b) \\
 F_{yz}(\xi_a, \eta_b) &= \beta_0 + \beta_1 \eta_b + \dots + \beta_{n-1} \eta_b^{n-1} + \beta_n \eta_b^n + \beta_{n+1} \xi_a^{2 \times 1} \\
 &\quad + \beta_{n+2} \xi_a^{2 \times 1} \eta_b + \dots + \beta_{2n} \xi_a^{2 \times 1} \eta_b^{n-1} + \dots \\
 &\quad + \beta_{l-2} \xi_a^{2(n-1)} + \beta_{l-1} \xi_a^{2(n-1)} \eta_b + \beta_l \xi_a^{2n} \\
 &= \sum_{i=0}^l \beta_i G_i(\xi_a, \eta_b) \\
 F_{zx}(\xi_a, \eta_b) &= \gamma_0 + \gamma_1 \xi_a \eta_b + \dots + \gamma_{n-1} \xi_a \eta_b^{n-1} + \gamma_n \xi_a \eta_b^n \\
 &\quad + \gamma_{n+1} \xi_a^{2 \times 1+1} + \gamma_{n+2} \xi_a^{2 \times 1+1} \eta_b + \dots \\
 &\quad + \gamma_{2n} \xi_a^{2 \times 1+1} \eta_b^{n-1} + \dots + \gamma_{l-2} \xi_a^{2(n-1)+1} \\
 &\quad + \gamma_{l-1} \xi_a^{2(n-1)+1} \eta_b + \gamma_l \xi_a^{2n+1} = \sum_{i=0}^l \gamma_i Q_i(\xi_a, \eta_b) \\
 l &= \sum_{k=0}^n (k+1) = \frac{(n+1)(n+2)}{2} \\
 G_0(\xi_a, \eta_b) &= 1, G_1(\xi_a, \eta_b) = \eta_b, \dots, G_{n+1}(\xi_a, \eta_b) \\
 &= \xi_a^{2 \times 1}, \dots, G_l(\xi_a, \eta_b) = \xi_a^{2n} \\
 Q_0(\xi_a, \eta_b) &= \xi_a, Q_1(\xi_a, \eta_b) = \xi_a \eta_b, \dots, Q_{n+1}(\xi_a, \eta_b) \\
 &= \xi_a^{2 \times 1+1}, \dots, Q_l(\xi_a, \eta_b) = \xi_a^{2n+1}
 \end{aligned} \right\} \quad (4)$$

The unknown coefficients $\alpha_0-\alpha_l, \beta_0-\beta_l, \gamma_0-\gamma_l$ are determined from the boundary conditions at suitably chosen collocation points [9].

3. Numerical results and discussion

3.1. Convergence of the results and satisfaction of boundary conditions

Numerical calculations have been carried out with varying n in Eq. (4) when $a/b = 1.0, 1.333, 1.5, 2.0, 4.0$ with Poisson's ratio $\nu = 0, 0.3, 0.45, 0.5$. Integrals in Eq. (3) have been evaluated numerically by applying a scientific subroutine library called the double-exponential-function-type formula. In demonstrating the numerical results of the stress intensity factors K_I, K_{II}, K_{III} the following

Table 2
Convergence of dimensionless stress intensity factors $F_{II}(\beta)$, $F_{III}(\beta)$, when $a/b = 1.0$, $\nu = 0.5$ in Fig. 1(c)

$\beta(\text{deg})/n$	1	2	3	4	5	6	7	8	9	10	15	20	25	
F_{II}	17	-0.06602	-0.04750	-0.03541	-0.02638	-0.01860	-0.01127	-0.00413	0.00283	0.00957	0.01607	0.04794	0.08367	0.12320
	18	-0.06652	-0.04804	-0.03607	-0.02704	-0.01913	-0.01161	-0.00430	0.00275	0.00952	0.01601	0.04784	0.08363	0.12317
	19	-0.06645	-0.04815	-0.03631	-0.02731	-0.01935	-0.01175	-0.00438	0.00269	0.00945	0.01590	0.04781	0.08365	0.12324
	20	-0.06638	-0.04835	-0.03667	-0.02768	-0.01964	-0.01194	-0.00449	0.00262	0.00938	0.01583	0.04779	0.08367	0.12330
F_{III}	17	0.07369	0.07273	0.07507	0.07899	0.08340	0.08773	0.09177	0.09551	0.09907	0.10256	0.12025	0.13590	0.14912
	18	0.07305	0.07239	0.07503	0.07915	0.08363	0.08795	0.09192	0.09560	0.09912	0.10260	0.12030	0.13586	0.14913
	19	0.07361	0.07259	0.07516	0.07927	0.08375	0.08801	0.09192	0.09556	0.09906	0.10255	0.12033	0.13582	0.14917
	20	0.07383	0.07278	0.07541	0.07956	0.08399	0.08819	0.09202	0.09560	0.09909	0.10259	0.12037	0.13579	0.14923
$\beta(\text{deg})/n$	30	35	40	45	50	55	60	65	70	75	80	85	90	
F_{II}	17	0.16714	0.21432	0.26395	0.31457	0.36487	0.41345	0.45884	0.49987	0.53509	0.56375	0.58481	0.59759	0.60192
	18	0.16713	0.21431	0.26396	0.31454	0.36485	0.41343	0.45887	0.49983	0.53511	0.56373	0.58480	0.59769	0.60199
	19	0.16712	0.21432	0.26395	0.31453	0.36487	0.41340	0.45885	0.49980	0.53513	0.56372	0.58478	0.59766	0.60193
	20	0.16711	0.21433	0.26392	0.31453	0.36486	0.41341	0.45882	0.49980	0.53512	0.56370	0.58479	0.59760	0.60189
F_{III}	17	0.15939	0.16597	0.16889	0.16757	0.16224	0.15278	0.13934	0.12227	0.10196	0.07896	0.05382	0.02727	0.00000
	18	0.15935	0.16602	0.16887	0.16757	0.16223	0.15276	0.13935	0.12225	0.10197	0.07897	0.05382	0.02723	0.00000
	19	0.15934	0.16603	0.16885	0.16763	0.16226	0.15276	0.13933	0.12225	0.10197	0.07896	0.05384	0.02725	0.00000
	20	0.15934	0.16604	0.16884	0.16767	0.16229	0.15277	0.13932	0.12225	0.10197	0.07897	0.05383	0.02726	0.00000

dimensionless factors F_I , F_{II} , F_{III} will be used

$$\left. \begin{aligned}
 F_I(\beta) &= \frac{K_I(\beta)}{\sigma_0^\infty \sqrt{\pi b}} = \frac{F_{zz}}{E(k)} \left[\sin^2 \beta + \left(\frac{b}{a}\right)^2 \cos^2 \beta \right]^{1/4} \\
 F_{II}(\beta) &= \frac{K_{II}(\beta)}{\tau_0^\infty \sqrt{\pi b}} = \left[F_{zx} \frac{k' \cos \beta}{B(k)} + F_{yz} \frac{\sin \beta}{C(k)} \right] \frac{k^2}{(1-k^2 \cos^2 \beta)^{1/4}} \\
 F_{III}(\beta) &= \frac{K_{III}(\beta)}{\tau_0^\infty \sqrt{\pi b}} = \left[-F_{zx} \frac{\sin \beta}{B(k)} + F_{yz} \frac{k' \cos \beta}{C(k)} \right] \frac{(1-\nu)k^2}{(1-k^2 \cos^2 \beta)^{1/4}}
 \end{aligned} \right\} \quad (5)$$

In addition, Murakami's $\sqrt{\text{area}}$ parameter is also applied when we consider the stress intensity factor at $\beta = \pi/2$ [12,13]. Here, 'area' is defined by Eq. (6)

$$\left. \begin{aligned}
 F_I^* &= K_I / \sigma_0^\infty \sqrt{\pi \sqrt{\text{area}}} \\
 F_{II}^* &= K_{II} / \tau_0^\infty \sqrt{\pi \sqrt{\text{area}}} \\
 F_{III}^* &= K_{III} / \tau_0^\infty \sqrt{\pi \sqrt{\text{area}}}
 \end{aligned} \right\} \quad (6)$$

$$\left[\begin{array}{ll}
 \text{ellipse: area} = \pi ab & \text{semi-ellipse: area} = \pi ab/2 \\
 \text{when } a/b \leq 0.2 & \text{when } a/b \leq 0.2 \\
 \text{area} = 20b^2 & \text{area} = 10b^2
 \end{array} \right]$$

It should be noted that for slender cracks such as $a/b \leq 0.2$ the crack area should be estimated as $\text{area} = 20b^2$ because the maximum stress intensity factor is almost independent of the real area of the crack. When Poisson's ratio $\nu = 0.5$, the corner point singular indices are $\lambda_S = 0.332$ and $\lambda_A = 0.646$ most different from the ordinary case 0.5. Therefore in Table 2, the convergence of the present results are shown with varying n when Poisson's ratio $\nu = 0.5$ in Fig. 1(c).

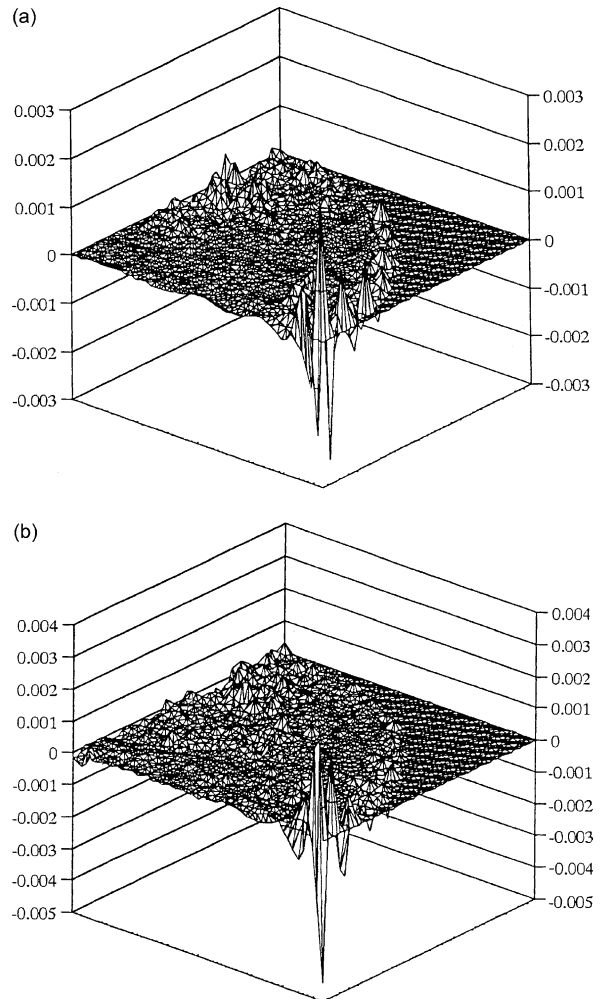


Fig. 4. Compliance of boundary condition when $a/b = 1.0$, $n = 20$, $\nu = 0.5$ in Fig. 1(c).

Table 3
Results of $F_{II}(\beta)$, $F_{III}(\beta)$ for a semi-elliptical crack when $\nu = 0.3$ in Fig. 1(c)

$\beta(\text{deg})/(alb)$	1	2	3	4	5	6	7	8	9	10	15	20	25	
F_{II}	1.00	-0.0737	-0.0540	-0.0405	-0.0300	-0.0207	-0.0123	-0.0043	0.0031	0.0100	0.0167	0.0490	0.0835	0.1207
	1.333	-0.0696	-0.0512	-0.0387	-0.0289	-0.0202	-0.0119	-0.0038	0.0041	0.0118	0.0193	0.0566	0.0970	0.1408
	1.50	-0.0666	-0.0486	-0.0365	-0.0271	-0.0187	-0.0107	-0.0027	0.0051	0.0129	0.0205	0.0591	0.1016	0.1475
	2.00	-0.0559	-0.0398	-0.0289	-0.0204	-0.0129	-0.0055	0.0020	0.0096	0.0174	0.0252	0.0659	0.1117	0.1612
	4.00	-0.0344	-0.0227	-0.0140	-0.0067	0.0001	0.0069	0.0141	0.0216	0.0294	0.0376	0.0806	0.1283	0.1797
F_{III}	1.00	0.0831	0.0887	0.0957	0.1025	0.1087	0.1142	0.1191	0.1238	0.1283	0.1329	0.1552	0.1744	0.1905
	1.333	0.0747	0.0772	0.0822	0.0880	0.0937	0.0990	0.1038	0.1082	0.1124	0.1166	0.1368	0.1534	0.1669
	1.50	0.0725	0.0735	0.0774	0.0823	0.0875	0.0923	0.0968	0.1010	0.1050	0.1090	0.1280	0.1436	0.1559
	2.00	0.0619	0.0608	0.0630	0.0668	0.0711	0.0756	0.0798	0.0838	0.0876	0.0911	0.1069	0.1197	0.1291
	4.00	0.0466	0.0423	0.0421	0.0435	0.0454	0.0476	0.0498	0.0519	0.0540	0.0559	0.0643	0.0706	0.0739
$\beta(\text{deg})/(alb)$	30	35	40	45	50	55	60	65	70	75	80	85	90	
F_{II}	1.00	0.1611	0.2042	0.2491	0.2947	0.3399	0.3835	0.4241	0.4607	0.4922	0.5176	0.5364	0.5479	0.5518
	1.333	0.1878	0.2366	0.2863	0.3357	0.3834	0.4284	0.4695	0.5060	0.5370	0.5618	0.5798	0.5906	0.5942
	1.50	0.1964	0.2470	0.2981	0.3485	0.3969	0.4424	0.4838	0.5204	0.5514	0.5762	0.5941	0.6051	0.6088
	2.00	0.2134	0.2666	0.3201	0.3722	0.4218	0.4682	0.5104	0.5476	0.5790	0.6041	0.6220	0.6330	0.6371
	4.00	0.2348	0.2894	0.3446	0.3983	0.4494	0.4969	0.5403	0.5787	0.6112	0.6372	0.6559	0.6672	0.6707
F_{III}	1.00	0.2024	0.2102	0.2132	0.2112	0.2040	0.1919	0.1748	0.1532	0.1277	0.0988	0.0673	0.0342	0.00000
	1.333	0.1762	0.1814	0.1821	0.1786	0.1708	0.1591	0.1436	0.1249	0.1034	0.0796	0.0541	0.0273	0.00000
	1.50	0.1641	0.1684	0.1684	0.1645	0.1568	0.1456	0.1311	0.1138	0.0941	0.0723	0.0491	0.0248	0.00000
	2.00	0.1348	0.1370	0.1360	0.1319	0.1248	0.1153	0.1034	0.0894	0.0737	0.0565	0.0383	0.0194	0.00000
	4.00	0.0766	0.0768	0.0757	0.0731	0.0686	0.0630	0.0563	0.0486	0.0399	0.0304	0.0206	0.0104	0.00000

As shown in Table 2, the results have good convergence to about the fourth digit even in the case $\nu=0.5$. Also, Fig. 4 indicates the compliance with the boundary conditions when $\nu=0.5$, $alb=1.0$, $n=20$, and $\sigma_z^\infty = \sigma_0 = 1$. The boundary stresses τ_{yz} , which should be 0, are less than 3×10^{-3} , and the stresses τ_{zx} are less than 5×10^{-3} even in the worst case $\nu=0.5$, where the effect of the corner point singularity is large.

3.2. Variations of stress intensity factors

Tables 3 and 4 indicate the results for a semi-elliptical crack subjected to shear loading in the y -direction. The results of a semi-elliptical crack subjected to tension or shear loading in the x -direction are indicated in our previous studies [9,10].

Table 4
Results of $F_{II}(\beta)$, $F_{III}(\beta)$ for a semi-elliptical crack when $alb = 1.0$ in Fig. 1(c)

$\beta(\text{deg})/\nu$	0	1	2	3	4	5	6	7	8	9	10	15	20	25	
F_{II}	0.0	-0.1092	-0.0755	-0.0544	-0.0401	-0.0291	-0.0197	-0.0112	-0.0032	0.0043	0.0113	0.0180	0.0499	0.0822	0.1162
	0.30	-	-0.0737	-0.0540	-0.0405	-0.0300	-0.0207	-0.0123	-0.0043	0.0031	0.0100	0.0167	0.0490	0.0835	0.1207
	0.45	-	-0.0681	-0.0496	-0.0374	-0.0281	-0.0199	-0.0121	-0.0046	0.0026	0.0094	0.0158	0.0482	0.0837	0.1226
	0.50	-	-0.0664	-0.0484	-0.0367	-0.0277	-0.0196	-0.0119	-0.0045	0.0026	0.0094	0.0158	0.0478	0.0837	0.1233
F_{III}	0.0	0.0680	0.0882	0.1050	0.1186	0.1294	0.1382	0.1457	0.1524	0.1587	0.1648	0.1708	0.1982	0.2214	0.2403
	0.30	-	0.0831	0.0887	0.0957	0.1025	0.1087	0.1142	0.1191	0.1238	0.1283	0.1329	0.1552	0.1744	0.1905
	0.45	-	0.0773	0.0776	0.0812	0.0860	0.0908	0.0953	0.0994	0.1033	0.1070	0.1108	0.1297	0.1461	0.1603
	0.50	-	0.0738	0.0728	0.0754	0.0796	0.0840	0.0882	0.0920	0.0956	0.0991	0.1026	0.1204	0.1358	0.1492
$\beta(\text{deg})/\nu$	30	35	40	45	50	55	60	65	70	75	80	85	90		
F_{II}	0.0	0.1526	0.1909	0.2304	0.2703	0.3097	0.3475	0.3826	0.4143	0.4414	0.4634	0.4796	0.4895	0.4929	
	0.30	0.1671	0.2042	0.2491	0.2947	0.3399	0.3835	0.4241	0.4607	0.4922	0.5176	0.5364	0.5479	0.5518	
	0.45	0.1656	0.2117	0.2600	0.3093	0.3582	0.4054	0.4495	0.4893	0.5235	0.5513	0.5717	0.5841	0.5882	
	0.50	0.2134	0.2143	0.2639	0.3145	0.3649	0.4134	0.4588	0.4998	0.5351	0.5637	0.5848	0.5976	0.6019	
F_{III}	0.0	0.2542	0.2629	0.2658	0.2627	0.2532	0.2377	0.2163	0.1894	0.1577	0.1220	0.0832	0.0422	0.00000	
	0.30	0.2024	0.2102	0.2132	0.2112	0.2040	0.1919	0.1748	0.1532	0.1277	0.0988	0.0674	0.0342	0.00000	
	0.45	0.1709	0.1779	0.1808	0.1794	0.1736	0.1633	0.1489	0.1307	0.1090	0.0844	0.0575	0.0291	0.00000	
	0.50	0.1593	0.1660	0.1688	0.1677	0.1623	0.1528	0.1393	0.1223	0.1020	0.0790	0.0538	0.0273	0.00000	

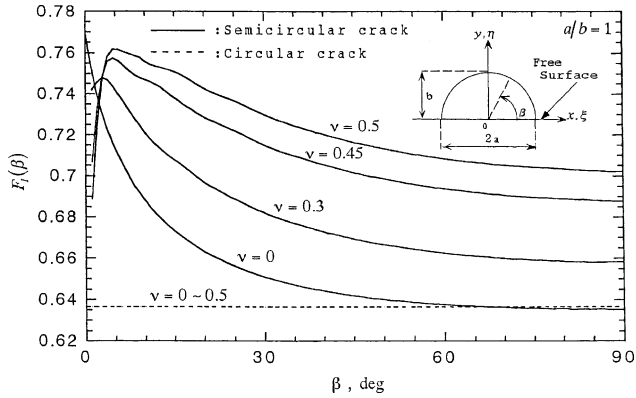


Fig. 5. Results for a semicircular crack $a/b = 1.0$ when $\nu = 0.0, 0.3, 0.45, 0.5$ in Fig. 1(a).

Figs. 5 and 6 indicate the results for a semi-elliptical crack under tension as shown in Fig. 1(a) for different Poisson's ratio and several elliptical ratios a/b in comparison with the results of an elliptical crack. In Fig. 5, K_I values of a semicircular crack at $\beta = 90^\circ$ are 8–10% larger than the values of a circular crack. The peak values of K_I appearing at $\beta = 3-5^\circ$ are 17–20% larger than the values of a circular crack. The K_I values at $\beta = 0^\circ$ should be zero except for the case of $\nu = 0$ because λ_S is less than 0.5. In Fig. 6, when $a/b \geq 1.5$, K_I has a maximum value at $\beta = 90^\circ$. With increasing a/b as $a/b = 1 \rightarrow \infty$, K_I values at $\beta = 90^\circ$ are 3–12% larger than the values of an elliptical crack.

Figs. 7 and 8 indicate the results of a semi-elliptical crack under shear in the x -direction for different Poisson's ratio and several elliptical ratios a/b in comparison with the results of an elliptical crack. In this case, with increasing a/b as $a/b = 1 \rightarrow \infty$, F_{III} values at $\beta = 90^\circ$ are 3–0% larger than the values of an elliptical crack. As $\beta \rightarrow 0^\circ$, $K_{II} \rightarrow \infty$ because λ_A is larger than 0.5. As $\beta \rightarrow 0^\circ$, K_{III} values should go to zero because $\tau_{yz} = 0$ at the free surface. However, K_{III} values do not go to zero smoothly as $\beta \rightarrow 0^\circ$ probably because of the effect of the corner point singularity $\lambda_A \geq 0.5$. The value of Poisson's ratio ν has a large effect on K_{III} values near the free surface.

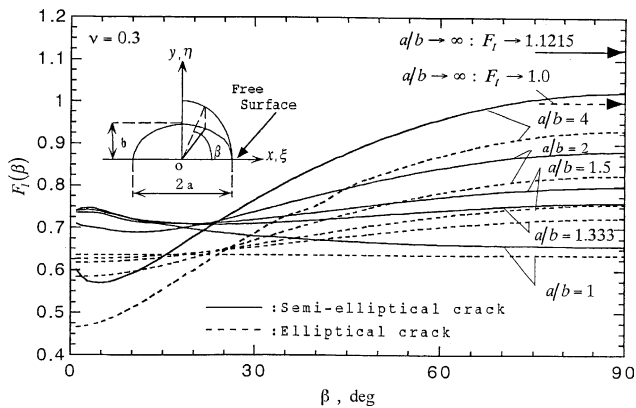


Fig. 6. Results for a semi-elliptical crack when $\nu = 0.3$ and $a/b = 1.0, 1.333, 1.5, 2.0, 4.0$ in Fig. 1(a).

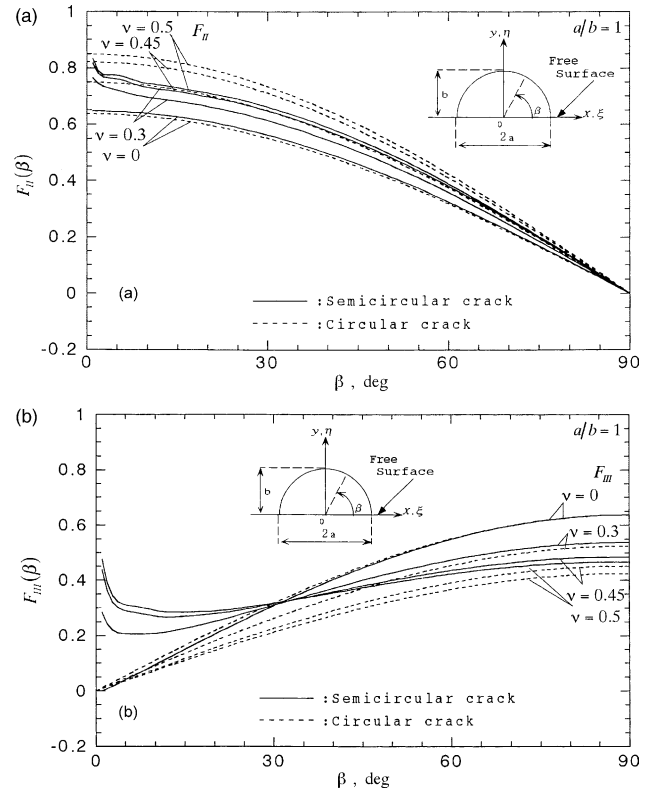


Fig. 7. Results for a semi-circular crack $a/b = 1.0$ when $\nu = 0.0, 0.3, 0.45, 0.5$ in Fig. 1(b) [(a) $F_{II}(\beta)$, (b) $F_{III}(\beta)$].

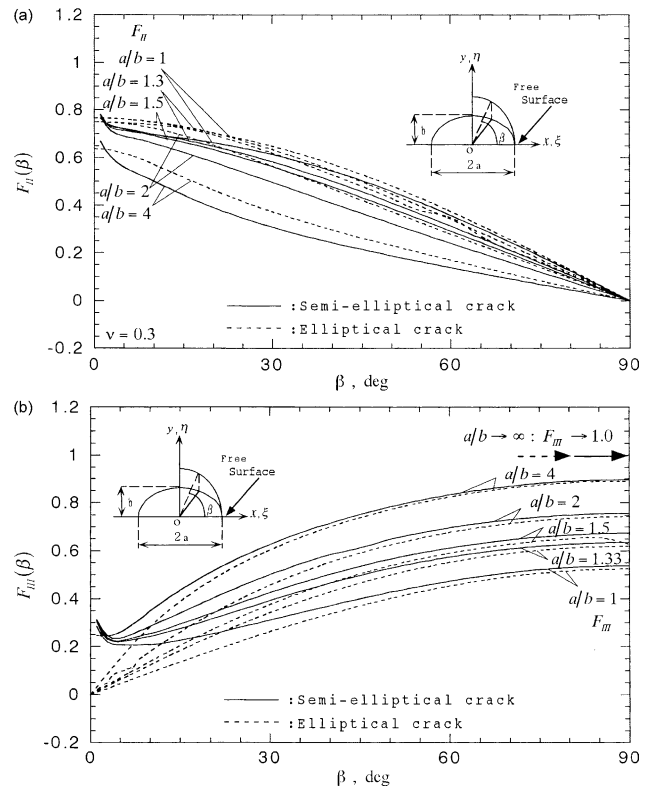


Fig. 8. Results for a semi-elliptical crack when $\nu = 0.3$ and $a/b = 1.0, 1.333, 1.5, 2.0, 4.0$ in Fig. 1(b) [(a) $F_{II}(\beta)$, (b) $F_{III}(\beta)$].

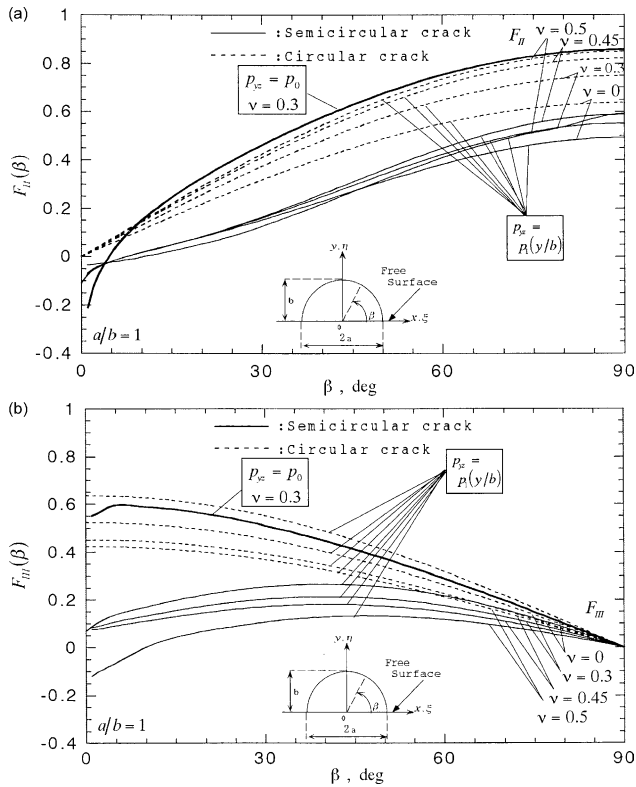


Fig. 9. Results for a semi-circular crack $a/b = 1.0$ when $\nu = 0.0, 0.3, 0.45, 0.5$ in Fig. 1(c) [(a) $F_{II}(\beta)$, (b) $F_{III}(\beta)$].

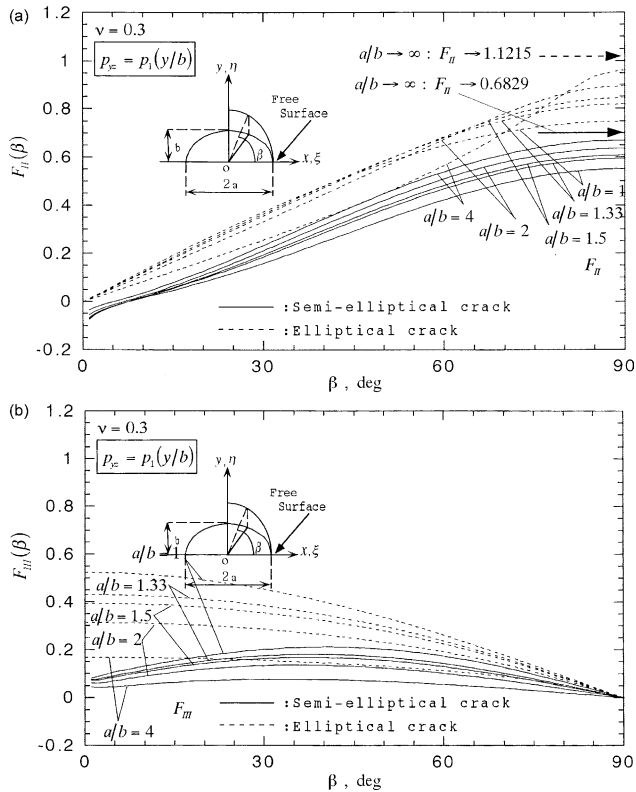


Fig. 10. Results for a semi-elliptical crack when $\nu = 0.3$ and $a/b = 1.0, 1.333, 1.5, 2.0, 4.0$ in Fig. 1(c) [(a) $F_{II}(\beta)$, (b) $F_{III}(\beta)$] (Results for $a/b \rightarrow \infty$ are indicated in [11]).

Table 5a

Results of K_I for an elliptical crack, a semi-elliptical crack, and a rectangular crack at A ($\nu = 0.3$)

	b/a			
	$p_{zz} = p_0,$ $p_{yz} = p_{zx} = 0$	$p_{zz} = p_0,$ $p_{yz} = p_{zx} = 0$	$p_{zz} = p_0,$ $p_{yz} = p_{zx} = 0$	$p_{zz} = p_0,$ $p_{yz} = p_{zx} = 0$
$\frac{K_{IA}}{p_{zz}\sqrt{\pi b}}$	1	0.6366	0.753	0.6585
	0.75	0.7239	–	0.7598
	2/3	0.7563	–	0.7983
	0.5	0.8257	0.906	0.8835
	0.25	0.9326	0.976	1.0234
	$\rightarrow 0$	1	1	1.1215
$\frac{K_{IA}}{p_{zz}\sqrt{\pi \sqrt{\text{area}}}}$	1	0.4781	0.533	0.5882
	0.75	0.5060	–	0.6315
	2/3	0.5133	–	0.6444
	0.5	0.5215	0.539	0.6636
	0.25	0.4953	0.489	0.6463
	$\rightarrow 0$	0.4728	0.472	0.6306

Figs. 9 and 10 indicate the results of a semi-elliptical crack under shear in the y -direction for different Poisson's ratio and several elliptical ratio a/b in comparison with the results of an elliptical crack under $p_{yz} = p_0$. In the case of a semi-elliptical crack under $p_{yz} = p_1(y/b)$, the K_{II} and K_{III} values are comparatively small because $p_{yz} \rightarrow 0$ as $\beta \rightarrow 0^\circ$. In particular, because $\tau_{yz} = 0$ at $y = 0$, K_{III} values are very different from the values of an elliptical crack.

3.3. Stress intensity factors at $\beta = 90^\circ$


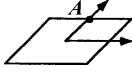

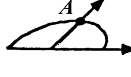
Tables 5a–5c indicate the results for stress intensity factors at $\beta = 90^\circ$ for an elliptical crack, a semi-elliptical crack, and a rectangular crack [12,13]. As shown in

Table 5b

Results of K_{II} for an elliptical crack, a semi-elliptical crack, and a rectangular crack at A ($\nu = 0.3$)

	b/a			
	$p_{zx} = p_0,$ $p_{zz} = p_{yz} = 0$	$p_{zx} = p_0,$ $p_{zz} = p_{yz} = 0$	$p_{zx} = p_0,$ $p_{zz} = p_{yz} = 0$	$p_{zx} = p_0,$ $p_{zz} = p_{yz} = 0$
$\frac{K_{IIIA}}{p_{zx}\sqrt{\pi b}}$	1	0.5243	0.654	0.5370
	0.75	0.6194	–	0.6348
	2/3	0.6571	–	0.6730
	0.5	0.7429	0.840	0.7566
	0.25	0.8915	0.953	0.8910
	$\rightarrow 0$	1	1	1
$\frac{K_{IIIA}}{p_{zx}\sqrt{\pi \sqrt{\text{area}}}}$	1	0.3938	0.462	0.4796
	0.75	0.4329	–	0.5276
	2/3	0.4460	–	0.5432
	0.5	0.4692	0.499	0.5683
	0.25	0.4734	0.476	0.5627
	$\rightarrow 0$	0.4728	0.473	0.5623

Table 5c
Results of K_{III} for an elliptical crack, a semi-elliptical crack, and a rectangular crack at A ($\nu = 0.3$)

	b/a	 $p_{yz} = p_0, p_{zx} = p_{zz} = 0$	 $p_{yz} = p_0, p_{zx} = p_{zz} = 0$	 $p_{yz} = p_0, p_{zx} = p_{zz} = 0$	 $p_{yz} = p_1(y/b), p_{zx} = p_{zz} = 0$
$\frac{K_{IIA}}{p_{yz}\sqrt{\pi b}}$	1	0.7490	0.841	0.8572	0.5517
	0.75	0.8202	–	–	0.5942
	2/3	0.8457	–	–	0.6088
	0.5	0.8956	0.955	–	0.6370
	0.25	0.9636	0.991	–	0.6706
	→ 0	1	1	1.1215*	0.6829*
$\frac{K_{IIA}}{p_{yz}\sqrt{\pi\sqrt{\text{area}}}}$	1	0.5625	0.594	0.7656	0.4928
	0.75	0.5733	–	–	0.4939
	2/3	0.5740	–	–	0.4914
	0.5	0.5656	0.567	–	0.4785
	0.25	0.5117	0.495	–	0.4236
	→ 0	0.4728	0.473	0.6306	0.3840

Tables 5a–5c, the normalized results by the root area parameter of an elliptical crack and rectangular crack are in good agreement independent of b/a . Therefore it may be concluded that the stress intensity factor at $\beta = 90^\circ$ can be expressed as shown in Eq. (7) in the range $b/a \leq 1$.

$$\left. \begin{aligned}
 &1. \text{ Under tension} \\
 &\text{Inside crack : } F_I^* = K_I/p_0\sqrt{\pi\sqrt{\text{area}}} = 0.50 \quad (0 < a/b < \infty) \\
 &\text{Surface crack : } F_I^* = K_I/p_0\sqrt{\pi\sqrt{\text{area}}} = 0.65 \quad (a/b > 1) \\
 &2. \text{ Under shear in the } x\text{-direction} \\
 &\text{Inside crack : } F_{III}^* = K_{III}/p_0\sqrt{\pi\sqrt{\text{area}}} = 0.45 \quad (a/b > 1) \\
 &\text{Surface crack : } F_{III}^* = K_{III}/p_0\sqrt{\pi\sqrt{\text{area}}} = 0.54 \quad (a/b > 1) \\
 &3. \text{ Under shear in the } y\text{-direction} \\
 &\text{Inside crack : } F_{II}^* = K_{II}/p_0\sqrt{\pi\sqrt{\text{area}}} = 0.54 \quad (a/b > 1) \\
 &\text{Surface crack : } F_{II}^* = K_{II}/p_1\sqrt{\pi\sqrt{\text{area}}} = 0.46 \quad (a/b > 1)
 \end{aligned} \right\} (7)$$

Eq. (7) are useful for evaluating the stress intensity factors of cracks with various shapes [14,15].

4. Conclusion

In this paper, a singular integral equation method is applied to calculate the stress intensity factor along the crack front of a 3D semi-elliptical surface crack in a semi-infinite body under tension in the z -direction and shear in the x - and y -directions as shown in Fig. 1. The body force

method is used to formulate the problem as a system of singular integral equations with singularities of the form r^{-3} using the stress field induced by a force doublet in a semi-infinite body as the fundamental solution. The conclusions are as follows.

- (1) For the tension problem as shown in Fig. 1(a), the mode I stress intensity factor K_I of a semicircular crack has a maximum value at $\beta = 3-5^\circ$ if Poisson's ratio $\nu \neq 0$. For semi-elliptical cracks in the range $a/b \geq 1.333$, the maximum K_I appears at $\beta = 90^\circ$. The value of K_I always goes to zero at $\beta = 0^\circ$ because the singular index λ_S at the corner point is less than 0.5 if Poisson's ratio $\nu \neq 0$ (see Figs. 5 and 6).
- (2) For the shear problem as shown in Fig. 1(b), the mode III stress intensity factors K_{III} of a semi-elliptical crack near the free surface are strongly affected by the corner point singularity if $\nu \neq 0$. The distributions of stress intensity factors become large especially near the free surface due to the effect of the corner point singularity. As $\beta \rightarrow 0^\circ$, K_{III} values should go to zero because $\tau_{yz} = 0$ at the free surface (see Figs. 7 and 8). However, the K_{III} values do not go to zero smoothly as $\beta \rightarrow 0^\circ$ even if $\nu \neq 0$.
- (3) For the shear problem as shown in Fig. 1(c), since $\tau_{yz} = 0$ at $y = 0$, K_{III} values are very different from the values of an elliptical crack (see Fig. 9). In the case of a semi-elliptical crack under $p_{yz} = p_1(y/b)$, the K_{II} and K_{III} values are comparatively small because $p_{yz} \rightarrow 0$ at $\beta \rightarrow 0^\circ$ (see Figs. 9 and 10).
- (4) Eq. (7) is useful for evaluating the stress intensity factors of a surface crack with arbitrary shape at the deepest point by using the $\sqrt{\text{area}}$ parameter.

References

- [1] Benthem JP. State of stress at the vertex of crack in a half-space. *Int J Solids Struct* 1977;13:479–92.
- [2] Benthem JP. The quarter-infinite crack in a half space; alternative and additional solutions. *Int J Solids Struct* 1980;16:119–30.
- [3] Bazant ZP, Estenssoro LF. Surface singularity and crack propagation. *Int J Solids Struct* 1979;15:405–26.
- [4] Takakuda K. Stress singularity at the crack tip of surface crack. *Trans JSME* 1984;50:1193–200. (in Japanese).
- [5] Pook LP. Some implications of corner point singularities. *Eng Fract Mech* 1994;48:367–78.
- [6] Murakami Y, Natsume H. Corner point singularity of 3-D crack subjected to mode II loading. *Trans JSME* 2000;66:2211–7. (in Japanese).
- [7] Otsuka A, Tohgo K, Yoshida M. Fatigue crack growth of a mixed three-dimensional crack (2nd report, fatigue crack growth behavior from a semi-elliptical surface crack under shear loading). *Trans JSME* 1987;54:1735–44. (in Japanese).
- [8] He MY, Hutchinson JW. Surface crack subject to mixed mode loading. *Eng Fract Mech* 2000;65:1–14.
- [9] Noda NA, Miyoshi S. Variation of stress intensity factor and crack opening displacement of semi-elliptical surface crack. *Int J Fract* 1996;75:19–48.
- [10] Noda NA, Kihara T, Beppu D. Analysis of variations of stress intensity factor of a semi-elliptical surface crack subjected to mixed mode loading. *Trans JSME* 2001;67:1542–7. (in Japanese).
- [11] Noda NA, Oda K. Numerical solutions of the singular integral equations in the crack analysis using the body force method. *Int J Fract* 1992;58:285–304.
- [12] Noda NA, Kihara TA. Variation of the stress intensity factor along the front of a 3-D rectangular crack subjected to mixed-mode load. *Arch Appl Mech* 2002;72:599–614.
- [13] Wang Q, Noda NA, Honda M, Chen MC. Variation of stress intensity factor along the front of a 3D rectangular crack by using a singular integral equation method. *Int J Fract* 2001;108:119–31.
- [14] Murakami Y, Endo M. Quantitative evaluation of fatigue strength of metals containing various small defects or cracks. *Eng Fract Mech* 1983;17-1:1–15.
- [15] Murakami Y. Analysis of stress intensity factors of modes I, II and III for inclined surface cracks of arbitrary shape. *Eng Fract Mech* 1985; 22-1:101–14.